THE EUROPEAN
PHYSICAL JOURNAL PLUS

Copepod swimming activity and turbulence intensity: study in the Agiturb turbulence generator system

Clotilde Le Quiniou[1], **François G. Schmitt**[1,a] (iD), **Enrico Calzavarini**[2,b] (iD), **Sami Souissi**[1,c] (iD), **Yongxiang Huang**[3,4,d] (iD)

[1] Université de Lille, CNRS, Univ. Littoral Côte d'Opale, UMR 8187 - LOG - Laboratoire d'Océanologie et de Géosciences, 62930 Wimereux, France
[2] Université de Lille, Unité de Mécanique de Lille - J. Boussinesq, ULR 7512, 59000 Lille, France
[3] State Key Laboratory of Marine Environmental Science, College of Ocean and Earth Sciences, Xiamen University, Xiamen 361102, China
[4] SMSE-Mingguang Joint Research Center for Advanced Palygorskite Materials, SJTU, Mingguang 239400, China

Abstract Copepods of the species *Acartia tonsa* have been placed in a laboratory generated turbulent flow system, called Agiturb, characterized by Taylor-scale-based Reynolds numbers from 130 to 360. Trajectories of alive and dead copepods, and of polystyrene spherical particles of size 600 μm, have been measured in the dark with infrared lights, using a high speed camera at 1200 fps. Using adequate filtering, horizontal velocity and acceleration measurements have been performed. The velocity probability density functions (PDF) of dead copepods are very close to the one of material particles of the same size. The PDFs of alive and dead copepods are different for low Reynolds numbers, and become superposed for Reynolds numbers larger than 160. On the contrary, the PDFs of accelerations of alive and dead copepods are also different for medium values of the Reynolds number, and become superposed for Reynolds numbers larger than 270. This shows that copepods' swimming behaviour occurs and is detectable under moderate turbulence, and not for high intensity turbulence. This gives information about the so called optimal turbulence levels for *Acartia tonsa* copepods and shows that when turbulence is of too high intensity, these copepods have no specific behavior.

1 Introduction

Turbulence is known to have important effects on marine ecosystems [1,2], and especially on plankton ecology [3–5], through a very efficient transport of dissolved matters, nutrients and particles. The influence of turbulence on zooplankton has been particularly studied, since it has been demonstrated to strongly increase the contact rate [6–9] which has importance for mating and for trophic interactions [10]. A too large turbulence intensity has however negative effects on the ingestion rate so that a dome-shape effect has been advocated for the influence of turbulence on zooplankton [11–13].

Copepods' behaviour has been studied in the field [14–17], but also intensively in the laboratory since the 1980s [10,18–23]. There have been many studies on the influence of turbulence on copepods swimming behaviour in the laboratory, using relatively low frame rate videos: from 15 frame per second (fps) to 100 or 125 fps [24,25]. However, copepods can swim very fast for their size, up to 50 cm/s, which is of the order of 1000 body size per second [21,26]. They can also develop huge accelerations during their jumps, up to 10-12 g [21,27], where g = 9.81 m/s² is the acceleration of gravity. The very rapid swimming and jumping events, associated to large velocities and accelerations, need for their detection high speed cameras. There are several references on copepod behaviour studies using high speed cameras [21,26–29], but all have been done in still water.

Here we present a pilot study of copepods' behaviour under turbulence, using a high speed camera with temporal resolution of the order tenths of milliseconds (0.8 ms) that can record in the infrared light. Copepods of the species *Acartia tonsa*, typical of estuaries and coastal zones, have been chosen. The next section presents the experimental device, called Agiturb, and the methodology for trajectory extraction and analysis. This is followed by a section presenting the first results, and a discussion.
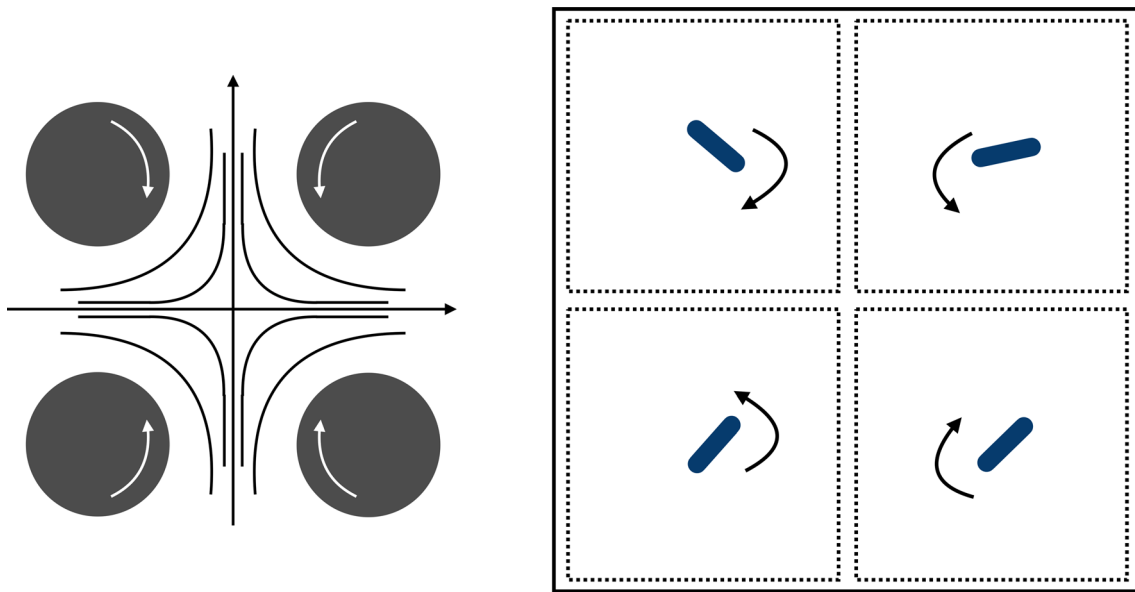
Fig. 1 **A** the flow generated by the four-roll mill [30] (adapted from [35]). **B** the geometry of agitator arrangement in our experiment, inspired by the four-roll mill flow

2 Material and methods

2.1 Generation of the turbulent flow

The turbulent flow is produced in the laboratory, using four contra-rotating agitators. The model for such flow is the so-called four-roll mill originally proposed in the 1930s by Taylor [30] to study drop deformation and break-up into smaller particles. It was designed to generate a laminar strain-dominated two-dimensional flow, by using four rolls having contra-rotating rotation rates (Fig. 1): it is now a classical flow that can be studied experimentally [31–34]. In our experiment, called "Agiturb", the flow close to the agitators is an unbounded flow similar to the four-roll mill, however without the cylindrical rolls. The injection of the energy in the flow is produced by 4 stirring bars (3.8 cm long with a diameter of 0.8 cm) activated by four magnetic stirrers (VELP MST Digital 5 L) situated at symmetric positions, the centers being placed at one-fourth of the width of the tank. The cubic tank (33.6 cm side) is made of flint glass (highly transparent) and is almost half-full with 15 L of sea water (see Fig. 2 and refer to Sect. 2.3 for details on sea water). For each experiment, the magnitude of the rotation rate Ω of each agitator was identical, with two agitators rotating clockwise and two anti-clockwise, the same directions being along the diagonal, see Fig. 1. Different values of Ω were chosen to reach different turbulence levels.

This flow is seeded by polystyrene particles or by copepods, depending on the experiments, and is observed using high speed cameras.

2.2 Video recordings with high-speed cameras

The flow is monitored using a high speed camera (Phantom C210) recording, from the bottom through a window, a plane layer at 3 cm from the bottom of the tank (Fig. 3). A 16 mm focal length Lens (FL-CC1614-2M, Ricoh lens) was used. The focus zone corresponds to a rectangular plane layer of 7×8.8 cm in the center of the aquarium with a width of $0.7 - 1$ cm. A horizontal two-dimensional (2D) projection of the trajectories is recorded, for particles belonging to this in focus volume, at an acquisition frequency of 1200 frames per second (300 μs exposure time) with 1280×1024 pixels (1.3 Mpixels). The camera is sensitive in the range 380–900 nm (quantum efficiency > 10%), and hence includes the infra-red. Two infrared light lamps (Raytec RAYMAX 25 10°, 850 nm) are fixed on each side of the aquarium in order to record the trajectories of alive copepods in the dark and prevent phototaxis, since *A. tonsa* has a very low visual sensitivity to red light [36]. The camera was linked to the PCC (Phantom Camera Control) software to record the videos (raw Cine format, 16bpp, 23 Go each video): 18 videos of about 7 s each were recorded to acquire 2 min of dataset for each experimental condition.

2.3 Aquaculture of *Acartia tonsa* copepods

Copepods that were studied belong to the *Acartia tonsa* species, typical of estuarine or shallow waters [37]. Their prosome length was measured with a mean of 600 ± 10 μm (Fig. 4). Mass culture of copepods were maintained in large transparent tanks (300–500 L)

Fig. 2 The experimental device, Agiturb, used to record copepods' trajectories in a turbulent flow generated by four agitators (with four stirring bars), a high speed camera beneath and two IR-lamps (on two vertical opposite sides of the tank)
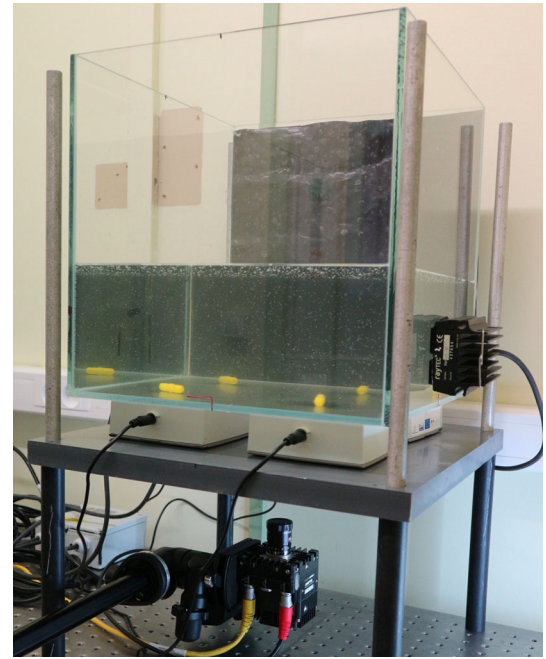
Fig. 3 Sketch of the experimental setup showing the position of the camera, the relative focus plane and the position of the stirrer, side view (**A**), top view (**B**). The red arrow indicates the distance L corresponding to the injection scale
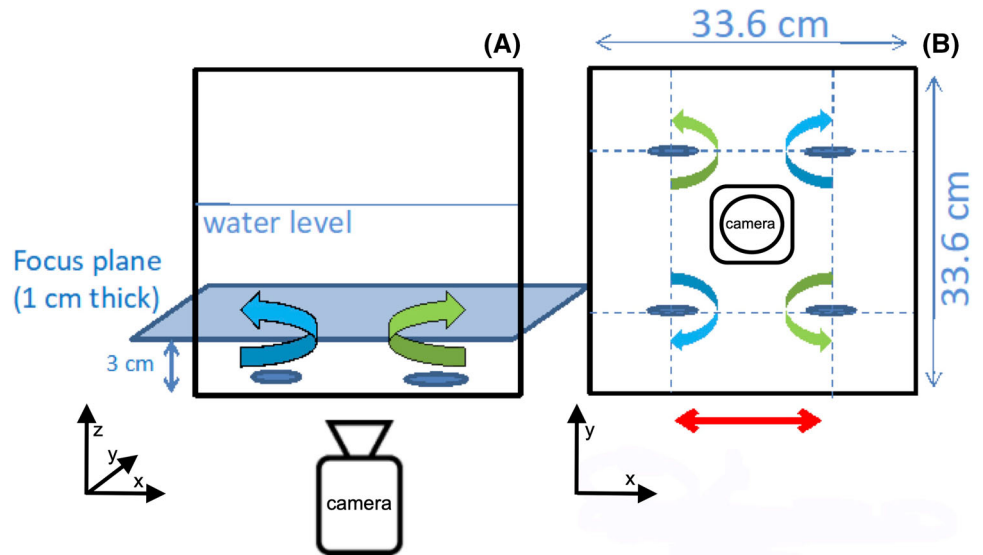
Fig. 4 One individual copepod of the *Acartia tonsa* species. *Source* C. Bialais, LOG

in similar conditions as described in [38,39]. Individuals are cultivated in the laboratory under day-night controlled light conditions and permanent oxygenation, in sea water at a temperature of 18–20°C. They are fed with the algae *Rhodomonas baltica*. In total, 60,000 copepods were necessary to acquire all the experimental conditions at a spatial density of 1 individual per cm³. Sea water used for the experiments is the one provided in marine station of the laboratory of Oceanology and Geosciences in Wimereux: it is coastal water from the Eastern English Channel, pumped and filtered. The salinity is in between 30 to 32 PSU. The water temperature during the experiments was ranging from 16.4°C to 19.5°C.

2.4 Sampling strategy

Different types of organisms have been successively added to the flow. In order to detect signs of swimming behavior, both alive and dead copepods in the dark have been considered. The initial pool of cultivated copepods was divided in different batches dedicated to specific turbulence intensities. Each batch of copepods was employed for recordings in still water and under two turbulence intensities to ensure they stayed healthy and in good shape during the measurement (we performed a phototaxis check before and after each measurement). Alive copepods were killed with 70% ethanol, rinsed and measured in the same experimental conditions of turbulence in which they were filmed alive. In order to detect the possible influence of particle shape, we also recorded trajectories of spherical particles with a close size and density as copepods (Synthos EPS® Expandable Polystyrene particles MP42W, 600 μm diameter and mass density of 1.05 g/cm³). Polystyrene particle were added at the same bulk density as the copepods (1 particle per cm³).

In this way, for still water we have recorded trajectories of swimming copepods, and for a given rotation rate, there are 3 categories of Lagrangian trajectories which will be compared: polystyrene particles, alive copepods and dead copepods. Mean values and probability density functions (PDF) are considered.

2.5 Flow characterization

Turbulence is characterized by Acoustic Doppler velocimetry (Vectrino Plus, Nortek) detecting the velocity of particles with a 8–13 μm mean diameter (Borosilicate glass particles of density 1.1 g/cm³, Potter industries) added to a concentration of 33 mg/L. The sampling volume is 5 cm distant from the probe and forms a cylinder of 6 mm diameter and 6.4 mm height. The probe is located in the center of the tank such that the sampling volume was 3 cm above the bottom of the tank. The sampling frequency is 200 Hz. Time series, containing 150,000 sampling points, were acquired at different turbulence intensities ranging from 100 to 900 rounds per minute (rpm).

Since the conditions are stationary, at a given spatial location the averages are performed in time ($\langle \cdot \rangle$ is a time average). We introduce the kinetic energy as $K = \frac{1}{2}(\sigma_{v_x}^2 + \sigma_{v_y}^2 + \sigma_{v_z}^2)$, where $V = (v_x, v_y, v_z)$ is the velocity vector, and σ^2 the variance. A mean fluctuating velocity $\tilde{u}$ can be introduced in relation with the kinetic energy as,

$$\tilde{u}^2 = \frac{2}{3}K \tag{1}$$

Next, in such system the energy is injected at a scale L which is of the order of the distance between the centers of two adjacent agitators (see Fig. 3). In our system we have $L = 16.8$ cm. From these two quantities, an estimation of the turbulent kinetic energy dissipation rate per unit mass (units $m^2 s^{-3}$) is the following [40]

$$\epsilon \sim \frac{\tilde{u}^3}{L} \tag{2}$$

From this, the Kolmogorov (or dissipative) scale η characterizing the scale of the smallest eddies is given by the following equation,

$$\eta = \left(\frac{\nu^3}{\epsilon}\right)^{1/4} \tag{3}$$

where for a mean temperature of 18 ± 2°C we take $\nu = 1.1 \times 10^{-6}\ m^2/s$ [2]. Via the relation for energy dissipation rate in developed turbulent flows (i.e. statistically homogeneous and isotropic) [40] $\epsilon = 15\nu\tilde{u}^2/\lambda^2$ provides the Taylor scale λ as,

$$\lambda = \sqrt{15}\eta^{2/3}L^{1/3} \tag{4}$$

The Taylor scale has no clear physical interpretation but is often used in the field of turbulence; as shows this equation, it is in between the Kolmogorov scale and the injection scale. From the Taylor scale, the Taylor-based Reynolds number is obtained:

$$Re_\lambda = \frac{\tilde{u}\lambda}{\nu} \tag{5}$$

In the fluid mechanics community, the Taylor-based (or microscale) Reynolds number Re_λ is preferred to the large-scale (or integral) Reynolds number $Re = UL/\nu$, where U is a mean velocity amplitude [41]. While the latter is based on the mean velocity, the former is based on the fluctuations with respect to the mean and it is a more general definition, because turbulent flow may

exist even in the absence of a mean flow current (when $U = 0$). Therefore, Re_λ permits the comparison between different types of turbulent flows, including direct numerical simulations and field studies [40].

All these parameters characterize the statistics of the turbulent flow which is produced, and may help to compare results obtained in this system with other turbulent flows in the field, in the laboratory or numerically produced.

2.6 Trajectory analysis and estimation of copepods horizontal velocity and acceleration

From the video recording to the estimation of the Lagrangian velocities, the different steps are explained below.

First, the positions of particles are identified on each image after background removing. The dynamics information from one frame to the other, and the identification of several moving particles as belonging to a single trajectory, are done through a Lagrangian tracking algorithm implemented using the Trackpy package written in Python. This algorithm is presented in "Appendix 1". It provides a collection of Lagrangian 2D trajectories in the form of successive positions $(x(t), y(t))$. Each trajectory does not necessarily have the same length. In practice, we have selected trajectories having lengths from 90 to 8264 frames, corresponding to 0.075 to 6.887 seconds.

The trajectories are recorded at high frequency (1200 fps), so that they can be assumed to be smooth enough for postprocessing analysis based on numerical differentiation. However, there are huge fluctuations in a turbulent flow and copepods may produce jumps with large velocities and accelerations. To compute the Lagrangian velocity and acceleration, smoothing and differentiation are done in the same step. The velocity is evaluated through a convolution of the trajectory with the derivative of a Gaussian kernel [42–44]. The width of the Gaussian kernel corresponds to a characteristic scale for the smoothing; the latter must be chosen both sufficient for the derivatives not to be influenced by small scale noise, and not too strong to keep significant variations of the signal occurring at the Kolmogorov scale. The procedure for the convolution and the choice of the adequate smoothing scale are presented in "Appendix 2".

3 Results

3.1 Characterization of the flow

Measurements of the flow velocity are done using the velocimeter, situated at the center of the device. The statistics are done over 150, 000 values, recorded during almost 13 minutes. From this, all three components of the turbulent velocity are recorded at 200 Hz, and the characteristic velocity $\tilde{u}$ is estimated. From this and using the above listed Eqs. (1–5), the dissipation ϵ, the Kolmogorov scale η and the Taylor scale λ are estimated, providing finally the Taylor-based Reynolds number Re_λ. These values are given in Table 1, and are represented in Fig. 5. We see that $\tilde{u}$ increases almost linearly with the stirring frequency, with values from about 1 to 6 cm/s (Fig. 5 a). The dissipation ϵ ranges from about 3×10^{-6} to 10^{-3} m^{2}s^{-3} (Fig. 5 b shown in a log-linear plot), which corresponds to values found in epicontinental seas to coastal zones [2,45]. The two length scales η and λ decrease with the rotation rate (Fig. 5 c shown in a log-linear plot) and finally the Taylor-based Reynolds number Re_λ increases almost linearly from a value of 134 ± 9 at 100 rpm, to a value of 356 ± 4 at 900 rpm (Fig. 5 d). The range of values of Re_λ found here are representative of moderate to high ocean turbulence intensities: fully developed turbulence requires values larger than 100, and Re_λ can reach 2×10^4 in tidal channels [46].

3.2 Velocity statistics: mean and PDF

Using the procedure presented above and detailed in Appendix 1 and 2, Lagrangian velocity is computed from the trajectories. This is done for several values of the rotation rate Ω, from $\Omega = 0$ to 900 rpm. In still water ($\Omega = 0$), only alive copepods are recorded.

Table 1 Values of different turbulent parameters as a function of the Agiturb stirring rotation rate Ω

Ω (rpm)	$\tilde{u}$ (cm/s)	ϵ (cm^2s^{-3})	η (mm)	Re_λ
100	0.78 ± 0.1	$2.8 \pm 1.2 \times 10^{-2}$	0.83 ± 0.08	134 ± 9
200	1.15 ± 0.1	$9.1 \pm 2.4 \times 10^{-2}$	0.62 ± 0.04	162 ± 7
250	1.43 ± 0.1	0.17 ± 0.04	0.53 ± 0.03	181 ± 7
300	1.86 ± 0.1	0.38 ± 0.06	0.43 ± 0.02	207 ± 3
400	2.51 ± 0.11	0.94 ± 0.12	0.34 ± 0.02	240 ± 5
500	3.19 ± 0.12	1.93 ± 0.2	0.29 ± 0.01	270 ± 5
550	3.48 ± 0.2	2.51 ± 0.25	0.27 ± 0.01	283 ± 5
700	4.31 ± 0.12	4.77 ± 0.4	0.23 ± 0.005	314 ± 5
900	5.52 ± 0.13	10.0 ± 0.7	0.19 ± 0.005	356 ± 4

The error bars are estimated from the velocity measurement systematic errors, which for the Vectrino device are reported by Nortek to be 0.5% + 1mm/s

Fig. 5 Properties of the flow at increasing flow stirring (in rpm: rounds per minute): **A** fluctuating velocity; **B** the dissipation ϵ; **C** Kolmogorov scale η; and **d** the Taylor-based Reynolds number R_λ
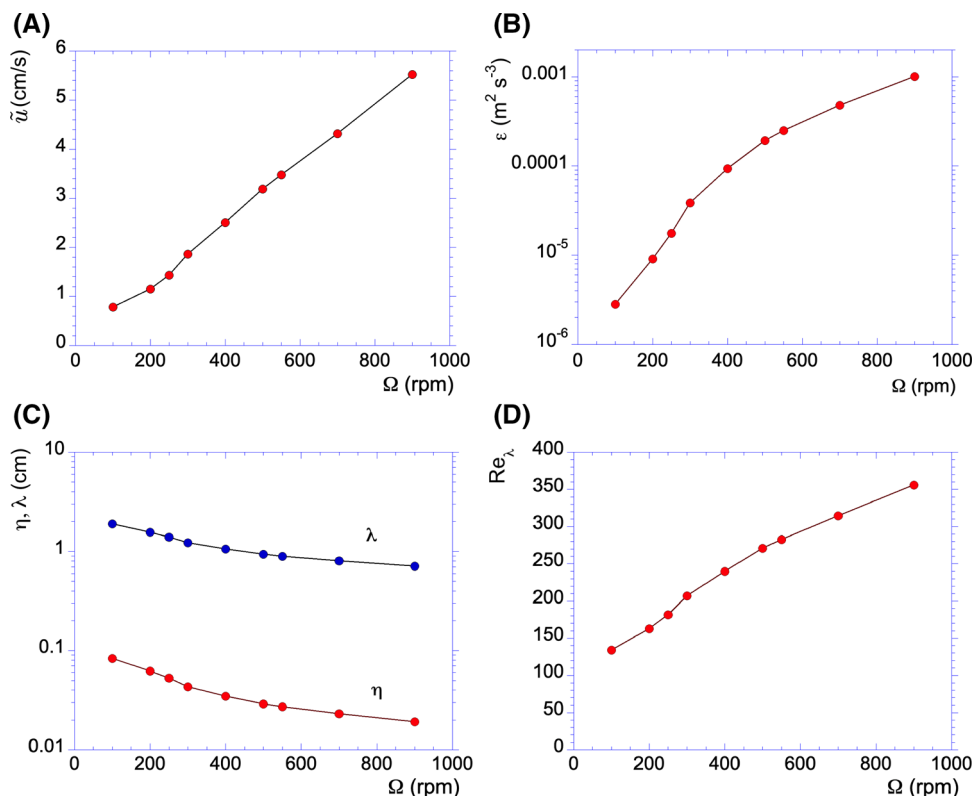

Fig. 6 Mean velocities versus rotation rate. Lagrangian horizontal velocities for dead copepods, alive copepods and spherical polystyrene particles are represented, together with the Eulerian fluctuating velocity estimated in the center of the flow. In still water, most of the time the copepods are not swimming. The mean velocity is close to zero, but if computed for events conditioned on a velocity larger than 1 mm/s, the mean velocity value (0.48 cm/s) is reported here as a yellow square
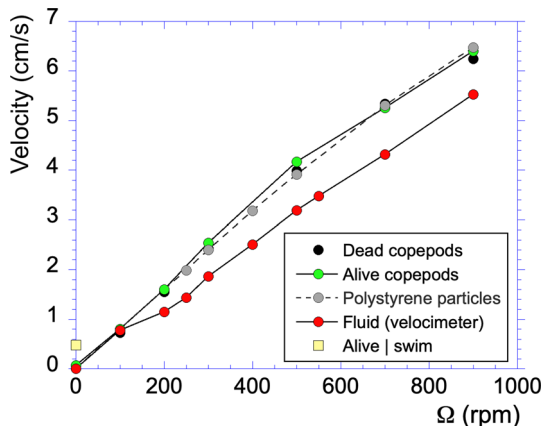
In this case, the measured Lagrangian velocity (v_x, v_y) corresponds to the swimming activity of copepods. For $\Omega = 100$ to 900 rpm, dead and alive copepods trajectories are recorded. In this case the estimated Lagrangian velocity is representative of the sum of turbulent advection and the possible swimming activity. For $\Omega > 250$ rpm, polystyrene particles are also recorded (for too low values of the rotation rate polystyrene particles did not mix enough in the flow and the experiment could not be exploited). This comparison is performed because if there is a statistical difference between dead copepods and spherical polystyrene particles of approximately the same size, this would possibly indicate an effect of the shape of the copepods.

Figure 6 presents the mean velocities (modulus of the Lagrangian horizontal velocity vector) versus the rotation rate. The numerical values and their statistical errors are given in Table 2. The fluid velocity $\tilde{u}$ (represented in Fig. 5 a) is also plotted for comparison. The latter is the Eulerian fluctuating velocity extracted at the center of the flow, using three components of the velocity vector, whereas the other plots (dead and alive copepods, and particle velocity) are the 2D Lagrangian velocity estimated over the whole measurement volume. It is visible that both velocities are comparable, and that no difference is evident for the different Lagrangian mean velocities. The mean velocity of swimming copepods in still water ($\Omega = 0$) is also estimated for nonzero velocities (a threshold of 1 mm/s is considered) since most of the time, copepods stays immobile. The mean swimming velocity is found to be $\bar{v} = \langle v|v > 0 \rangle = 0.48$ cm/s (the conditional average notation here is meant to correspond to a temporal average of nonzero swimming velocity, since copepods are often immobile in still water).

Table 2 Mean values and standard deviation of the Lagrangian velocities (in cm/s) of alive copepods, dead copepods, and polystyrene particles, as a function of the Agiturb stirring rotation rate Ω

Ω (rpm)	Alive copepods	Dead copepods	Particles
100	0.80 ± 0.4	0.73 ± 0.37	–
200	1.60 ± 0.8	1.55 ± 0.8	–
300	2.54 ± 1.2	2.42 ± 1.2	2.40 ± 1.2
500	4.17 ± 2	3.99 ± 2	3.91 ± 2
700	5.25 ± 2.7	5.34 ± 2.8	5.30 ± 2.8
900	6.4 ± 3.3	6.24 ± 3.2	6.47 ± 3.4

For small rotation rates (< 300 rpm), particles were not mixed efficiently, staying at the surface and their data could not be recorded

Fig. 7 Probability density functions of the Lagrangian horizontal velocity amplitude estimated for still water (no turbulence) corresponding to swimming activity of copepods (red), and for a rotation rate of $\Omega = 100$ rpm, for dead (gray) and alive copepods (green)
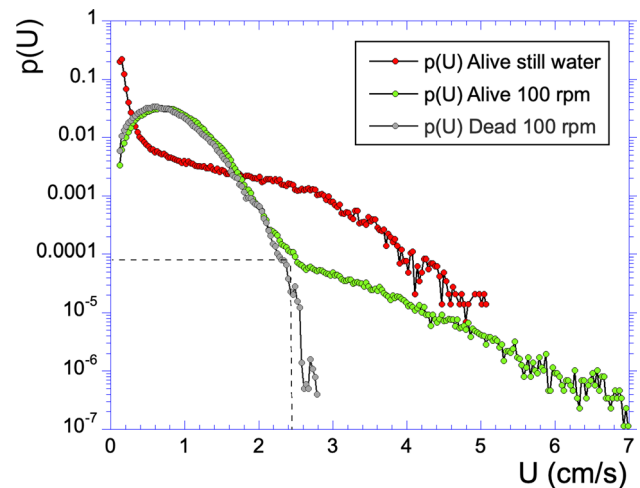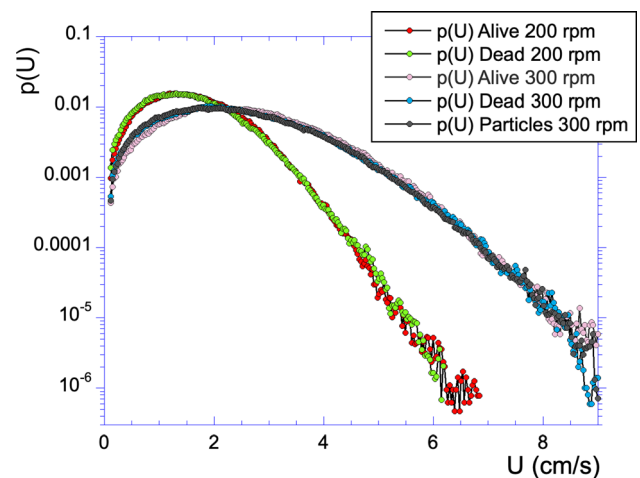

Fig. 8 PDF of 2D Lagrangian velocity modulus for rotation rates $\Omega = 200$ and 300 rpm, for alive and dead copepods, and also (for $\Omega = 300$ rpm only) for spherical polystyrene particles

As a next step, we consider the probability density functions of the Lagrangian velocities: it may be that the mean value is comparable while differences are visible on the PDF. Figure 7 represents the PDF of the swimming velocity modulus of copepods in still water $U = \sqrt{v_x^2 + v_y^2}$, compared with the PDF of alive and dead copepods velocities at a low rotation rate ($\Omega = 100$ rpm). The PDF of the swimming velocity has a heavy tail. For velocities $U < 2.5$ cm/s, the PDF of dead and alive copepods nicely superpose, whereas for velocities $U > 2.5$ cm/s, the PDF of alive copepods is very different from the dead ones, indicative of a swimming activity. This difference is no more visible for larger rotation rates (and hence larger turbulence intensities): Fig. 8 compares the PDF of alive and dead copepods for $\Omega = 200$ and 300 rpm, and also (for $\Omega = 300$ rpm only) for spherical polystyrene particles. The PDFs are very nicely superposed, except for the largest values, which are scattered due to poor sampling. Such behaviour is also found for larger values of the rotation rate (not shown here).

It is also visible that the PDFs of the velocity modulus get broader when turbulence intensity increases: this is shown for alive PDFs only in Fig. 9, for $\Omega = 200$ to 900 rpm. The range of values of the velocities increase with the rotation rate. In each case, there is a local maximum of the PDF, which also increases with the rotation rate.

Fig. 9 PDF of 2D Lagrangian velocity modulus for rotation rates $\Omega \geq 200$ rpm, for alive copepods
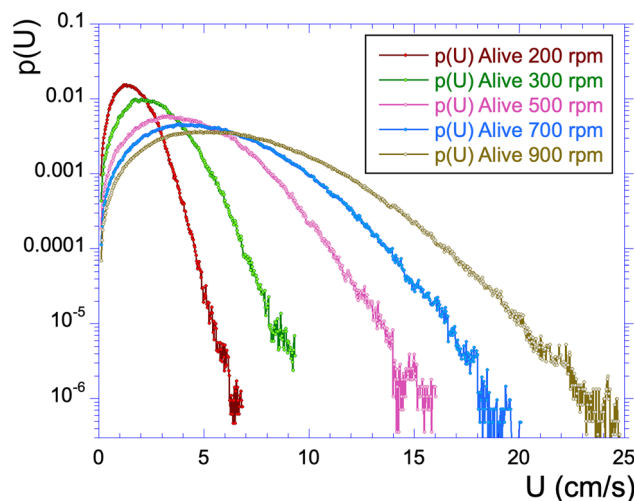

Fig. 10 Mean values of the Lagrangian horizontal acceleration intensity $a = \sqrt{a_x^2 + a_y^2}$, estimated for different impeller rotation rates, and displayed for the dead copepods (black symbols), alive copepods (green circles) and spherical polystyrene particles (grey circles). The yellow square represents the mean acceleration conditioned on nonzero swimming copepods (the threshold for this is as done above for the velocity, at 1 mm/s)
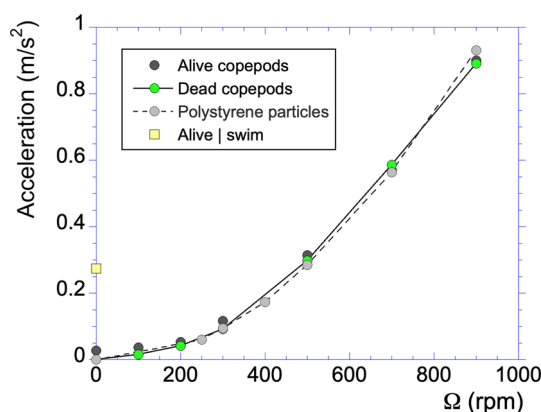
3.3 Acceleration statistics: mean and PDF

We then consider the horizontal acceleration statistics. Figure 10 shows the mean acceleration estimated for the different rotation rates, for dead copepods, alive copepods and spherical polystyrene particles. The numerical values and their statistical errors are given in Table 3. The mean values are very similar. In still water, the alive copepods acceleration is representative of the swimming behaviour. The mean acceleration is also estimated for swimming portions of the trajectories (the threshold is the same as in Fig. 6, i.e. for events for which the swimming velocity is larger than 1 mm/s).

The PDFs are also estimated, to detect possible changes in large values of the accelerations, even if the mean values do not show a difference. Figure 11 shows the PDF of 2D Lagrangian acceleration modulus in still water (no turbulence), and for the rotation rate $\Omega = 100$ rpm. There is a heavy tail for the accelerations values in still water. A very clear difference is found between the PDF of alive and dead copepods at rotation rate of 100 rpm, for acceleration larger than a small threshold of about $10\,\mathrm{cm\,s^{-2}}$. Contrary to the velocity case, this difference is still visible at 200 and 300 rpm, as found in Fig. 12. In the same figure, it is found that the dead copepods and spherical particles have very close PDFs at 300 rpm.

This difference between alive and dead copepods Lagrangian acceleration is almost vanishing at 500 rpm, and is no more visible at larger rotation rates and turbulence intensities (700 and 900 rpm), see Fig. 13.

4 Discussion

The Agiturb system generates turbulence intensities characterized mainly by the dissipation rate ϵ and the microscale Reynolds number Re_λ. For rotation rates going from $\Omega = 100$ to 900, we reach in the laboratory turbulence levels representative of the epicontinental seas (for low rotation rates) to coastal waters (for the largest rotation rates) [46]. Using such system, we could record the trajectories of alive and dead copepods and spherical polystyrene particles.

Several studies have characterized the behavior of copepods by considering statistics on the swimming speed and acceleration. Most of these studies were using a video camera whose speed was between 30 and 100 fps [25,47] and very few were performed using a high speed camera in still water [26,28,48,49], or under hydrodynamic stimuli [21,27,50,51]. Time resolution of the camera

Table 3 Mean values and standard deviation of the Lagrangian accelerations (in m/s^2) of alive copepods, dead copepods, and polystyrene particles, as a function of the Agiturb stirring rotation rate Ω

Ω (rpm)	Alive copepods	Dead copepods	Particles
100	0.037 ± 0.1	0.016 ± 0.02	–
200	0.053 ± 0.09	0.041 ± 0.04	–
300	0.117 ± 0.17	0.092 ± 0.09	0.094 ± 0.09
500	0.314 ± 0.29	0.298 ± 0.28	0.285 ± 0.27
700	0.57 ± 0.49	0.586 ± 0.54	0.564 ± 0.52
900	0.90 ± 0.75	0.891 ± 0.76	0.931 ± 0.8

For small rotation rates (< 300 rpm), particles were not mixed efficiently, staying at the surface and their data could not be recorded. The error bars are large compared with mean values, due to the large spreading of the Lagrangian acceleration data
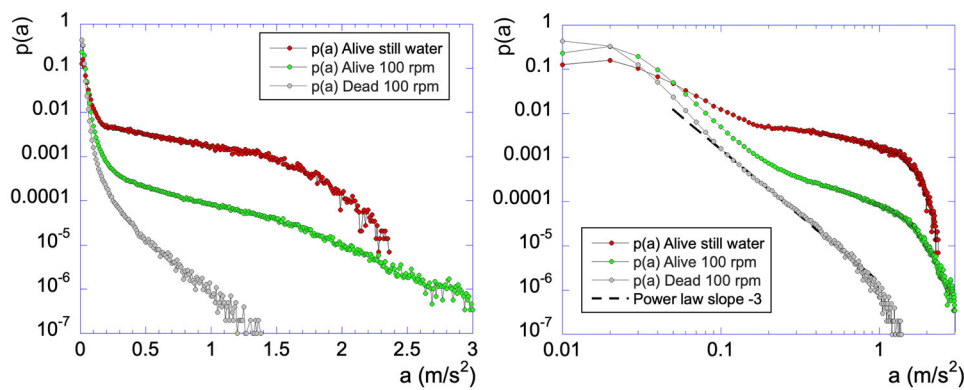

Fig. 11 PDF of the Lagrangian horizontal acceleration modulus in still water (no turbulence), and for the rotation rate $\Omega = 100$ rpm. Left: in log-linear plot, and right, in log-log plot. The log-log plots emphasizes the behaviour of the PDF for low acceleration values. A power-law fit of slope -3 is superposed to the PDF of dead copepods

and the procedure to derive velocity and acceleration from the tracks, can change the final value of the jump speed by a factor of 3 [25,49]. We used in our study a high speed camera (1200 fps) and a well tested signal processing procedure [42,43] in order to resolve properly short time scales in a quantitative way. The high speed camera is able to record with infrared light and to avoid phototaxis, since *A. tonsa* has a very low visual sensitivity to red light [36].

In our study, we have chosen a very common species of copepods, *Acartia tonsa*, that is reported to be especially sensitive to shear [52] and to vorticity when turbulence is high enough [53,54]. Compared to other species that by contrast swim cruising, *A. tonsa* swims in a hop-sink manner which makes it easier to detect and quantify changes of behavior [50,53,55]. We first found that, when considering mean quantities, no effect is visible since alive and dead copepods have very similar mean velocities (Fig. 6) and accelerations (Fig. 10). In Fig. 6 the fluid velocity cannot be directly compared to Lagrangian mean velocities of particles, since it is an estimate of the typical fluctuations of the turbulent fluctuations. Nevertheless, it is of the same order. The fact that the mean velocity and accelerations do not show differences in the dead and alive copepods can be seen as surprising; it is due mainly to the fact that the main differences, when there is a difference, is visible for large values of the velocities and accelerations, as shown by the PDFs (Fig. 7 for the velocity and Figs. 11 and 12 for the acceleration). This is compatible with previous studies that showed that *Acartia tonsa* copepods react to large values of the surrounding strain rate in turbulent flows [24,56]. In the latter work, where 3D copepods trajectories were recorded using particle image velocimetry (PIV) in a complex flow, it was found that 80% of the copepods responded to large strain flows only.

The PDF of alive and dead copepods for $\Omega = 100$ rpm identified a threshold of 2.5 cm/s: below this threshold both velocities were identical, showing that there is no clear swimming activity. Above this threshold, there is a very clear swimming activity that could be due to jump events. The acceleration threshold found in Figs. 11 and 12 are of the order of 0.1 (for $\Omega = 100$ rpm) to 0.6 ms^{-2} (for $\Omega = 300$ rpm). The fact that the rotation threshold for detecting swimming activity is different for the velocity and for the acceleration is also of interest: for Reynolds numbers between 160 and 270, the PDF of the velocity of dead and alive copepods is identical, but there is still a huge difference in the accelerations PDFs. We interpret this as a signature of localized jumps. The copepods at these rather important turbulent levels stop continuous swimming but have still intermittent jumps. This may indicate that too high values of the ambient turbulence are felt as harmful and copepods stop jumping to avoid fatigue. It confirms results obtained previously with the same species [24].

Fig. 12 PDF of Lagrangian horizontal acceleration modulus for the rotation rate $\Omega = 200$ rpm (alive and dead copepods), and for $\Omega = 300$ rpm (alive and dead copepods, and spherical polystyrene particles)
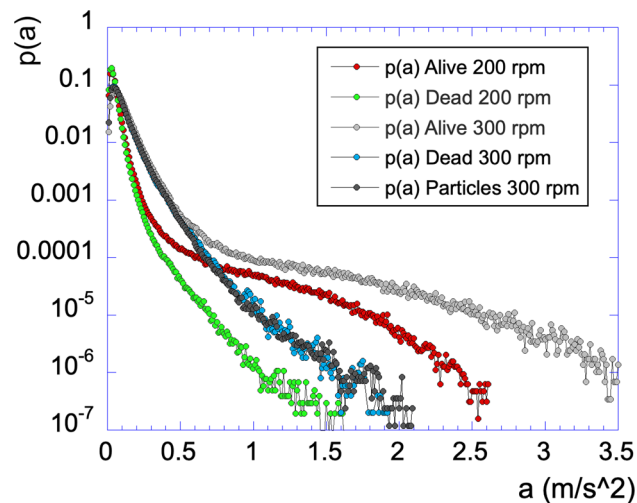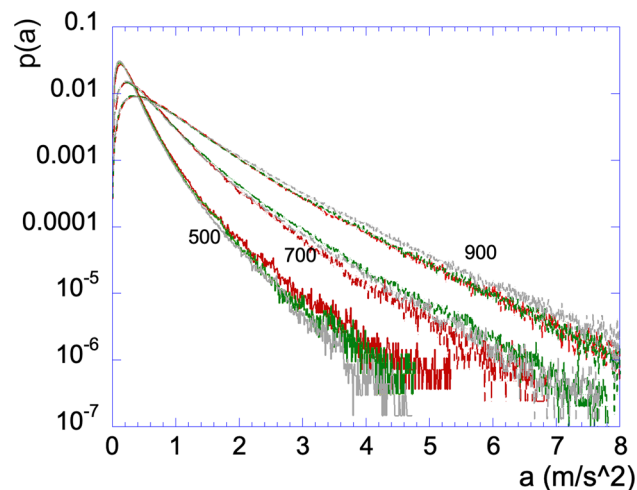

Fig. 13 PDF of Lagrangian horizontal acceleration modulus for the rotation rate $\Omega = 500, 700$ and 900 rpm: alive copepods are in red color, dead copepods in green and particles in grey

5 Conclusion and perspectives

We have presented here a new device for generating controlled turbulence in the laboratory, called Agiturb, and inspired by the four-roll mill flow proposed in 1934 by Taylor [30]. This flow has been characterized in terms of fundamental turbulence quantities such as the kinetic energy K, the dissipation of kinetic energy ϵ, the Kolmogorov scale η and the microscale Reynolds number Re_λ. The dependence of these quantities in terms of rotation rate Ω have been provided. The experiments done here range from $\Omega = 100$ to 900 rpm, reaching microscale Reynolds numbers from about 130 to 350, corresponding to medium to rather large situations of turbulence, found in the epicontinental seas and in the coastal regions. This Agiturb system is rather simple to build, and may serve as a model system for turbulent flow generation in the laboratory for further studies.

Turbulence is producing important fluid and particle accelerations at small scales [42], and copepods may jump with also large acceleration values. This shows that the study of their swimming and jumping behaviour need high speed cameras. Here for the first time we have considered a high speed camera system placed into turbulence, in the dark with an infrared light imaging capabilities at 1200 fps. This permits a precise estimation of the velocity and accelerations of copepods. The comparison with dead copepods in the same conditions helps to discriminate swimming activities.

Here it has been used for the first time with copepods of the species *Acartia tonsa*, typical of estuarine or coastal waters. Placed into the system at rest, it was found that their swimming velocity has a mean of about 0.5 cm/s. It was also shown that at moderate turbulence levels, copepods showed swimming activities. For Reynolds numbers between 160 and 270, copepods seem to stop swimming but have still localized jumps. At high turbulence level, this activity was no more visible, showing that copepods feel the ambient turbulence as too large. This is in favour of the hypothesis that there is an optimal turbulence window, from low turbulence to Reynolds numbers of about 270, among which copepods of the species *Acartia tonsa* have swimming and jumping activities. It corresponds to the optimal turbulence hypothesis also called "dome shape" effect [10–13]. In previous studies, this dome shape was a hypothesis mainly developed in models, and verified indirectly in the field. Here we have a direct experimental evidence of this dome.

This dome effect is very likely depending on the zooplankton species, and future studies could be proposed with the objective to compare the dome for different species. We have not considered the influence of food in the flow. Copepods were fed before the experiments. Swimming behaviour of *A. tonsa* is strongly influenced also by the food searching [57–60] and further studies may also consider how the dome effect is modified by the food concentration in the flow. Other applications of such system are mating efficiency.

We have focused here on PDFs of velocity and accelerations. We did not exploit the dynamical information contained in the trajectories. Since we have here Lagrangian trajectories, the intermittency [61,62] of copepods trajectories will be studied in future works, in order to detect possible swimming behaviour in the Lagrangian multiscale intermittent structures. Finally, we may indicate one important improvement of our Agiturb system: we have considered here the 2D projections of the velocity and accelerations. The synchronization of two or more high-speed cameras will be needed to reconstruction fully 3D trajectories. This will be an important next step of such studies.

**Data Availability Statement** This manuscript has associated data in a data repository.

6 Appendix 1: Particle tracking and trajectory extraction

In this appendix, the tracking algorithm is presented. It allows the extraction of particles successive positions, from the video images recorded at 1200 fps using the high speed camera. As a first step, the background is subtracted to the videos corresponding to the same turbulence intensity. In each case, the background is acquired while agitation was running without particles.

The tiny spots in video images, corresponding to copepods or particles, can be followed according to relevant parameters specifying their size, separation and intensity. A threshold is applied to automatically detect, for each frame, all particles. In order to detect only particles situated in the focal plane (a plane about 1 cm thick, Fig. 3), a maximum intensity is set to the 1% percentile, and the threshold is set to 35% of the maximum intensity. After finding features, a refinement provides sub-pixel precision coordinates by means of a least-squares fitting with a radial model function able to locate the center of brightness. To link the coordinates in time, from one frame to the other, a prediction framework is used, that relates the coordinates that are the closest in space and that have matching displacement directions. The center of brightness was allowed to move from one image to another with a maximum velocity of 50 cm/s (search range of 6 pixels considering the pixel/meter coefficient which is 68.4 µm/pixel).

A given particle is allowed to disappear from the tracking only for one image, and in this case during the post-processing an interpolation of the missing value is done from the two neighbored values. During a video sequence, many particles can be detected simultaneously, and finally individual particle trajectories are recorded. Only trajectories where the particle was travelling at least 30 pixels in one direction or another were selected (and example is shown in Fig. 14).

Fig. 14 A snapshot of detected particles (red dots) and their full trajectory reconstructed with the Trackpy Python package
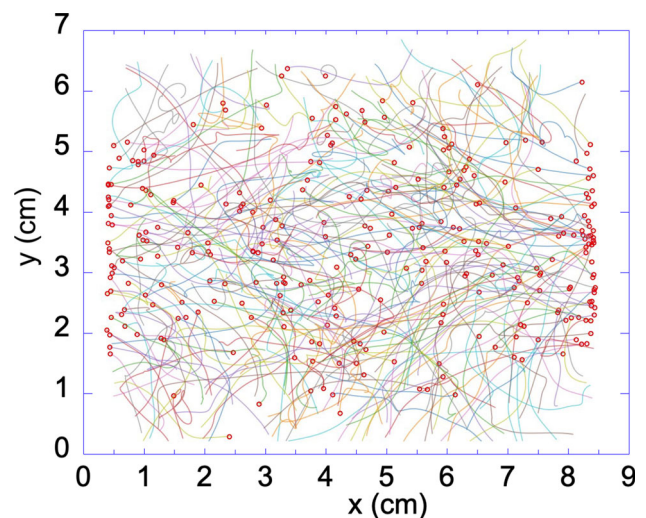
7 Appendix 2: Estimation of Lagrangian velocity and accelerations using a convolution with a Gaussian-based kernel

To calculate Lagrangian velocity and acceleration from the reconstructed horizontal trajectories, a convolution with a Gaussian-based kernel is performed. This kernel is based on the Gaussian PDF with a width of ω:

$$g(\tau) = \frac{1}{\omega\sqrt{\pi}} \exp\left(-\frac{\tau^2}{\omega^2}\right) \tag{6}$$

The Lagrangian velocity is estimated by performing a convolution of the trajectory with the derivative of this kernel [43,44]:

$$g_1(\tau) = -\frac{2\tau}{\omega^3\sqrt{\pi}} \exp\left(-\frac{\tau^2}{\omega^2}\right) \tag{7}$$

The acceleration is obtained from a convolution with the second derivative of the kernel:

$$g_2(\tau) = \frac{2}{\omega^3\sqrt{\pi}} \left(\frac{2\tau^2}{\omega^2} - 1\right) \exp\left(-\frac{\tau^2}{\omega^2}\right) \tag{8}$$

In practice the convolution is done locally, i.e. the kernel is set to 0 when $|\tau| > 3\omega$. Such truncation needs a slight linear correction to the kernels, which is found by stating that the kernel g_1 convoluted with the x function must give the value 1, and convolution of the kernel g_2 with the x^2 function must give the value 2.

Furthermore, the value of ω must be chosen. If ω is too large, there is too much smoothing and the true velocity and acceleration are minored. If too small, small-scale noise and errors in measurement may lead to spurious large values of the velocity and acceleration. An objective way to estimate this value is to vary ω and estimate the acceleration variance for each value of ω. When it is too low, the acceleration variance will diverge. This is illustrated in Fig. 15 for the 900 rpm case. The filtering time scale $\tau_f = \sqrt{2}\omega$ is normalized by the Kolmogorov time scale $\tau_\eta = (\nu/\epsilon)^{1/2}$. The acceleration variance is modelled by a power law when the filter length gets close to 0 [42,44]. When ω corresponds to 15 points, the ratio τ_f/τ_η goes from 0.075 at 250 rpm and 0.6 at 900 rpm: this choice corresponds to the scale below which the acceleration variance is diverging.

The filtering time scale is hence modified for each turbulence intensity (different values for each rotation rate). This is done for each trajectory, so that a database of Lagrangian velocity and acceleration time series is obtained. Some examples are shown in Fig. 16: the x, y positions during a series of three jumps are shown together with the corresponding velocities and accelerations. This illustrates the sporadicity of jumps, which last around 50 ms. This shows that a sampling frequency of the order to 1000 fps is needed to resolve correctly these copepod jump events. However, to resolve the most "explosive" jump events, a larger sampling frequency might be necessary.

Fig. 15 Effect of the filter length ω relative to the Kolmogorov time scale $\tau_\eta = (\nu/\epsilon)^{1/2}$ obtained from the Vectrino measurement, on the acceleration variance $< a_y'^2 >$ when applying the convolution of the kernel g_2 to the trajectories of polystyrene particles under 900 rpm
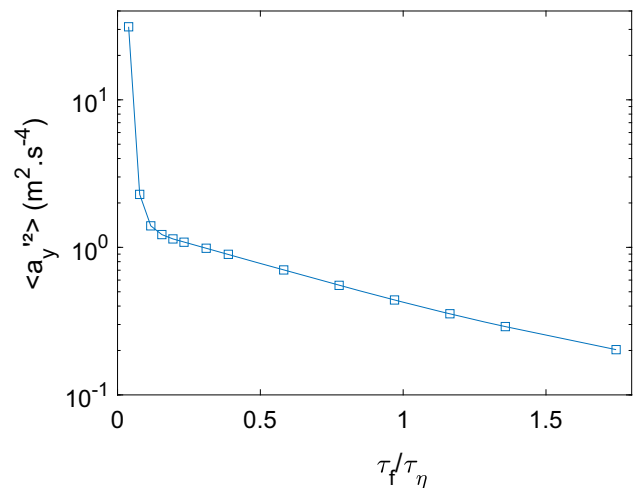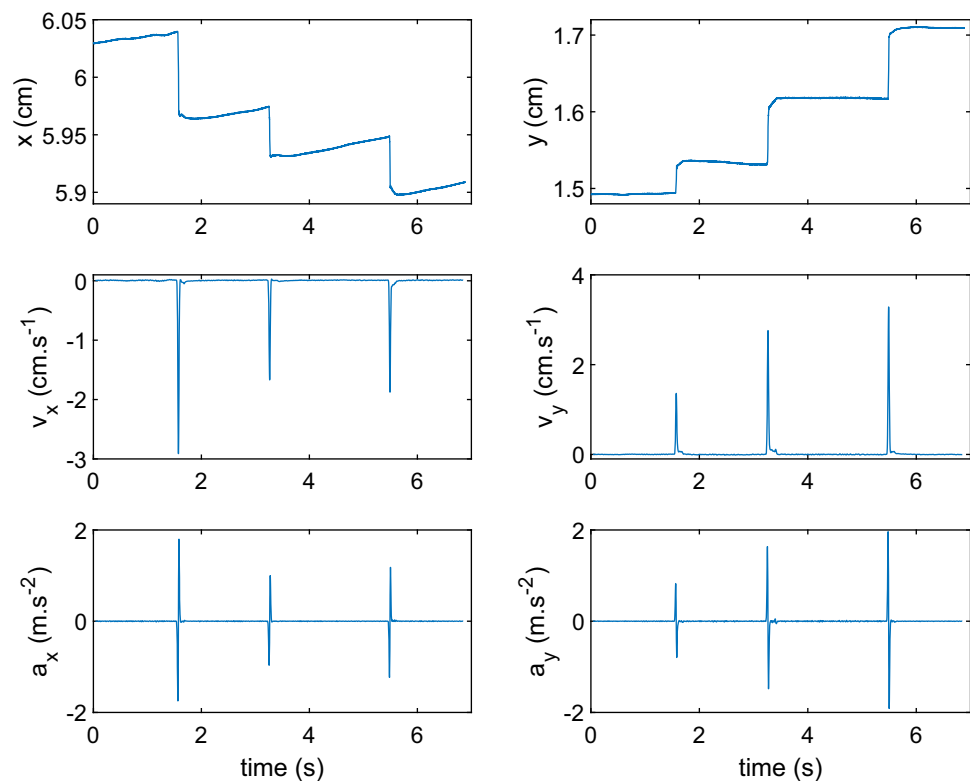
Fig. 16 Coordinates of the two-dimensional numerically reconstructed trajectory of one copepod that jumped three consecutive times and leading to the characteristic spikes in the velocity and acceleration signals

References

1. R. Margalef, Sci. Mar. **61**(Suppl 1), 109 (1997)
2. F.G. Schmitt, *Turbulence et écologie marine* (Ellipses, 2020)
3. M. Estrada, E. Berdalet, Sci. Mar. **61**(supl. 1), 125 (1997)
4. F. Peters, C. Marrasé, Mar. Ecol. Prog. Ser. **205**, 291 (2000)
5. P.A. Jumars, J.H. Trowbridge, E. Boss, L. Karp-Boss, Mar. Ecol. **30**(2), 133 (2009)
6. B.J. Rothschild, T.R. Osborn, J. Plankton Res. **10**(3), 465 (1988)
7. H. Pécseli, J. Trulsen, Ø. Fiksen, Prog. Oceanogr. **101**(1), 14 (2012)
8. H.L. Pécseli, J.K. Trulsen, Ø. Fiksen, Limnol. Oceanogr. Fluids Environ. **4**(1), 85 (2014)
9. H. Ardeshiri, F.G. Schmitt, S. Souissi, F. Toschi, E. Calzavarini, J. Plankton Res. **39**(6), 878 (2017)
10. T. Kiørboe, *A Mechanistic Approach to Plankton Ecology* (Princeton University Press, Princeton, 2008)
11. P. Cury, C. Roy, Can. J. Fish. Aquat. Sci. **46**(4), 670 (1989)
12. S. Sundby, P. Fossum, J. Plankton Res. **12**(6), 1153 (1990)
13. B.R. MacKenzie, T.J. Miller, S. Cyr, W.C. Leggett, Limnol. Oceanogr. **39**(8), 1790 (1994)
14. Y. Lagadeuc, M. Bouté, J.J. Dodson, J. Plankton Res. **19**(9), 1183 (1997)
15. A.W. Visser, H. Saito, E. Saiz, T. Kiørboe, Mar. Biol. **138**(5), 1011 (2001)
16. L.S. Incze, D. Hebert, N. Wolff, N. Oakey, D. Dye, Mar. Ecol. Prog. Ser. **213**, 229 (2001)
17. R.E. Fontana, M.L. Elliott, J.L. Largier, J. Jahncke, Prog. Oceanogr. **142**, 1 (2016)
18. E.J. Buskey, Mar. Biol. **79**(2), 165 (1984)
19. T. Kiørboe, E. Saiz, M. Viitasalo, Mar. Ecol. Prog. Ser. **143**, 65 (1996)
20. D.M. Fields, J. Yen, J. Plankton Res. **24**(8), 747 (2002)
21. R.J. Waggett, E.J. Buskey, Mar. Biol. **150**(4), 599 (2007)
22. M. Moison, F.G. Schmitt, S. Souissi, L. Seuront, J.S. Hwang, J. Mar. Syst. **77**(4), 388 (2009)
23. L. Sabia, M. Uttieri, F.G. Schmitt, G. Zagami, E. Zambianchi, S. Souissi, Zool. Stud. **53**(1), 1 (2014)
24. O.M. Gilbert, E.J. Buskey, J. Plankton Res. **27**(10), 1067 (2005)
25. F.G. Michalec, S. Souissi, M. Holzner, J. R. Soc. Interface **12**(106), 20150158 (2015)
26. E.J. Buskey, D.K. Hartline, Biol. Bull. **204**(1), 28 (2003)
27. E.J. Buskey, P.H. Lenz, D.K. Hartline, Mar. Ecol. Prog. Ser. **235**, 135 (2002)
28. T. Kiørboe, A. Andersen, V.J. Langlois, H.H. Jakobsen, T. Bohr, Proc. Natl. Acad. Sci. **106**(30), 12394 (2009)
29. T. Kiørboe, A. Andersen, V.J. Langlois, H.H. Jakobsen, J. R. Soc. Interface **7**(52), 1591 (2010)
30. G.I. Taylor, Proc. R. Soc. Lond. Ser. A **146**(858), 501 (1934)
31. B.J. Bentley, L.G. Leal, J. Fluid Mech. **167**, 219 (1986)
32. B. Andreotti, S. Douady, Y. Couder, J. Fluid Mech. **444**, 151 (2001)
33. S. Wereley, L. Gui, Exp. Fluids **34**(1), 42 (2003)
34. F. Akbaridoust, J. Philip, I. Marusic, Meas. Sci. Technol. **29**(4), 045302 (2018)
35. R.R. Lagnado, L.G. Leal, Exp. Fluids **9**(1), 25 (1990)

36. D.E. Stearns, R.B. Forward, Mar. Biol. **82**(1), 85 (1984)
37. J.H.S. Blaxter, B. Douglas, P.A. Tyler, J. Mauchline, *The Biology of Calanoid Copepods* (Academic Press, Cambridge, 1998)
38. Y.J. Pan, E. Déposé, A. Souissi, S. Hénard, M. Schaadt, E. Mastro, S. Souissi, Aquac. Res. **51**(7), 3054 (2020)
39. Y.J. Pan, W.L. Wang, J.S. Hwang, S. Souissi, Front. Mar. Sci. p. 1386 (2021)
40. S.B. Pope, *Turbulent Flows* (Cambridge University Press, Cambridge, 2000)
41. H. Tennekes, J.L. Lumley, *A First Course in Turbulence* (MIT Press, Cambridge, 1972)
42. G.A. Voth, A. La Porta, A.M. Crawford, J. Alexander, E. Bodenschatz, J. Fluid Mech. **469**, 121 (2002)
43. N. Mordant, E. Lévêque, J.F. Pinton, New J. Phys. **6**(1), 116 (2004)
44. R. Ni, S.D. Huang, K.Q. Xia, J. Fluid Mech. **692**, 395 (2012)
45. T.C. Granata, T.D. Dickey, Prog. Oceanogr. **26**(3), 243 (1991)
46. J. Jimenez, Sci. Mar. **61**(suppl. 1), 47 (1997)
47. T. Kiørboe, E. Saiz, A. Visser, Mar. Ecol. Prog. Ser. **179**, 97 (1999)
48. T. Kiørboe, J. Plankton Res. **33**(5), 677 (2011)
49. H. Ardeshiri, I. Benkeddad, F.G. Schmitt, S. Souissi, F. Toschi, E. Calzavarini, Phys. Rev. E **93**(4), 043117 (2016)
50. L.A. van Duren, J.J. Videler, J. Exp. Biol. **206**(2), 269 (2003)
51. T. Kiørboe, H. Jiang, R.J. Gonçalves, L.T. Nielsen, N. Wadhwa, Proc. Natl. Acad. Sci. **111**(32), 11738 (2014)
52. D.M. Fields, J. Yen, J. Plankton Res. **19**(9), 1289 (1997)
53. D.R. Webster, D.L. Young, J. Yen, Integr. Comp. Biol. **55**(4), 706 (2015)
54. D. Elmi, D.R. Webster, D.M. Fields, J. Exp. Biol. **224**(3), jeb237297 (2021)
55. G. Dur, S. Souissi, F.G. Schmitt, F.G. Michalec, M.S. Mahjoub, J.S. Hwang, Hydrobiologia **666**(1), 197 (2011)
56. D. Adhikari, B.J. Gemmell, M.P. Hallberg, E.K. Longmire, E.J. Buskey, J. Exp. Biol. **218**(22), 3534 (2015)
57. E. Saiz, M. Alcaraz, G.A. Paffenhöfer, J. Plankton Res. **14**(8), 1085 (1992)
58. P. Tiselius, Limnol. Oceanogr. **37**(8), 1640 (1992)
59. E. Saiz, Limnol. Oceanogr. **39**(7), 1566 (1994)
60. E. Saiz, T. Kiørboe, Mar. Ecol. Prog. Ser. **122**, 147 (1995)
61. F.G. Schmitt, L. Seuront, Physica A **301**(1–4), 375 (2001)
62. F.G. Michalec, F.G. Schmitt, S. Souissi, M. Holzner, Eur. Phys. J. E **38**(10), 1 (2015)